

# Stability of the kinematically coupled $\beta$ -scheme for fluid-structure interaction problems in hemodynamics

Sunčica Čanić<sup>a,\*</sup>, Boris Muha<sup>a</sup>, Martina Bukač<sup>a</sup>

<sup>a</sup>*Department of Mathematics, University of Houston, Houston, Texas 77204-3476*

---

## Abstract

It is known that classical Dirichlet-Neumann loosely coupled partitioned schemes for fluid-structure interaction (FSI) problems are unconditionally unstable for certain combinations of physical and geometric parameters that are relevant in hemodynamics. It was shown by Causin, Gerbeau, and Nobile [17] that these instabilities are associated with the “added-mass effect”. The “added mass effect” was studied in [17] by considering the simplest FSI problem which captures the main features responsible for the instabilities of classical Dirichlet-Neumann loosely coupled schemes. By considering the same test problem, the present work shows that a novel, partitioned, loosely coupled scheme, recently introduced in [11], called the kinematically coupled  $\beta$ -scheme, does not suffer from the added mass effect for any  $\beta \in [0, 1]$ , and is unconditionally stable for all the parameter values in the problem. Numerical results are presented for a fully nonlinear benchmark FSI problem in hemodynamics of Formaggia et al. [30]. The results show that the scheme is stable for this benchmark problem even for the parameter values well within the parameter range for which the classical Dirichlet-Neumann schemes are unconditionally unstable. The main contribution of this work is in explicitly showing how the implicit enforcement of the kinematic coupling condition and the inclusion of the structure inertia into the fluid sub-problem avoid the presence of the added mass effect in the kinematically-coupled  $\beta$ -scheme.

**Keywords:** Fluid-structure interaction, Partitioned schemes, Stability analysis, Added-mass effect

---

\*Corresponding author

*Email addresses:* canic@math.uh.edu (Sunčica Čanić), borism@math.hr (Boris Muha), martina@math.uh.edu (Martina Bukač)

---

## 1. Introduction

Fluid-structure interaction (FSI) problems have important applications in various areas including bio-fluids and aero-elasticity. They have been extensively studied from the numerical, as well as analytical point of view [5, 7, 8, 9, 10, 18, 19, 20, 22, 23, 27, 29, 31, 35, 37, 38, 39, 40, 43, 44, 45, 49, 50]. A set of popular numerical schemes for FSI in blood flow includes partitioned schemes (loosely or strongly coupled). Partitioned schemes typically solve an underlying multi-physics problem by splitting the problem into sub-problems determined by the different physics in the coupled problem. In particular, in fluid-structure interaction problems the fluid dynamics and structure elastodynamics are often solved using separate solvers. In loosely coupled schemes only one iteration between the fluid and structure sub-problem is performed in each time step, while in strongly coupled schemes several sub-iterations between the fluid and structure sub-problems need to be performed at each time step to achieve stability.

The main advantages of *loosely coupled partitioned schemes* are modularity, simple implementation, and low computational costs. However, in [17] it was proved that for certain combinations of physical and geometric parameters (which are realistic in blood flow) “classical” Dirichlet-Neumann loosely coupled schemes are unconditionally unstable. In the same paper, the authors showed that this instability is due to the “added-mass effect”. Namely, it was shown that a portion of the fluid load to the structure in the coupled FSI problems can be written as an additional inertia term in the structure equation coming from the fluid mass (added mass). In numerical schemes in which this term appears *explicitly*, which is the case in the classical Dirichlet-Neumann loosely coupled partitioned schemes, the added mass term acts as a source of instabilities when the structure is too “light” to counter-balance the kinetic energy of the “heavy” fluid load.

To get around these difficulties, several different loosely coupled algorithms have been proposed. The method proposed in [5] uses a simple membrane model for the structure which can be easily embedded into the fluid problem where it appears as a generalized Robin boundary condition. In this way the original problem reduces to a sequence of fluid problems with a generalized Robin boundary condition which can be solved using only the fluid solver. A similar approach was proposed in [43] where the fluid and structure

were split in the classical way, but the fluid and structure sub-problems were linked via novel transmission (coupling) conditions that improve the convergence rate. Namely, a linear combination of the dynamic and kinematic interface conditions was used to artificially redistribute the fluid stress on the interface, thereby avoiding the difficulty associated with the added mass effect.

A different approach to stabilization of loosely coupled (explicit) schemes was proposed in [15]. There, a stabilization based on Nitsche’s method [34] was used with a time penalty term giving an  $L^2$ -control on the fluid force variations at the interface. We further mention the scheme proposed in [6] where a Robin-Robin type preconditioner was combined with Krylov iterations for a solution of an interface system.

For completeness, we also mention several semi-implicit FSI schemes. The schemes proposed in [26, 1, 2] separate the computation of fluid velocity from the coupled pressure-structure velocity system, thereby reducing the computational costs. Similar schemes, derived from algebraic splitting, were proposed in [3, 47]. We also mention [41] where an optimization problem is solved at each time-step to achieve continuity of stresses and continuity of velocity at the interface.

Recently, a novel loosely coupled partitioned scheme, called the “kinematically coupled  $\beta$ -scheme”, was introduced in [11]. This scheme successfully deals with problems associated with the added mass effect in a way different from those reported above. The kinematically coupled  $\beta$ -scheme is a modification of the kinematically coupled scheme first introduced in [33]. The parameter  $\beta$  was introduced in [11] to increase the accuracy. This parameter distributes the fluid pressure between the fluid and the structure sub-problems. For  $\beta = 0$  the entire pressure is considered in the fluid sub-problem giving no pressure loading in the structure sub-problem, while for  $\beta = 1$ , the entire fluid pressure is used to load the structure sub-problem. The case  $\beta = 0$  corresponds to the classical kinematically coupled scheme [33].

The first version of the scheme, presented in [11], concerns FSI problems in which the structure is described by a thin structure model (a thin membrane or shell model; elastic or viscoelastic). Extensions of the scheme have recently been developed by the authors to handle FSI problems with thick structures modeled by the equations of 2D or 3D elasticity [13], and to handle FSI problems with multiple layered structures (thin-thick-thin-thick. . . ; elastic or viscoelastic) [14]. Modeling FSI with multi-layered structures is particularly

useful in the blood flow application since the walls of major arteries are composed of several layers: the *tunica intima*, the *tunica media*, and the *tunica adventitia*, separated by the thin elastic laminae.

Recently, the authors have used the kinematically-coupled scheme to prove the existence of a weak solution to a fully nonlinear FSI problem between an incompressible, viscous fluid and a thin structure modeled by either the elastic or viscoelastic shell equations [40]. The existence proof is based on constructing approximate solutions using the kinematically-coupled scheme, and showing that the approximate solutions converge to a weak solution as the time-discretization tends to zero. This existence result relies on energy estimates which show that in the kinematically-coupled scheme the energy of the coupled FSI problem is well-approximated by the discretized problem. A consequence of this result is that the kinematically-coupled scheme is stable. The stability of the kinematically coupled scheme is achieved by a clever splitting of the structure problem into the inertia part (combined with the viscoelastic part when the (thin) structure is viscoelastic) and the elastic part. The structure inertia is then used as a boundary condition in the fluid sub-problem, while the elastodynamics part is solved separately. The inclusion of the structure inertia (and possibly the viscoelastic part of a thin structure) into the fluid sub-problem was enabled by an implicit enforcement of the kinematic coupling condition, which enforces the no-slip condition at the fluid-structure interface.

The present manuscript reveals, explicitly, how and why the kinematically-coupled  $\beta$ -scheme does not suffer from the added mass effect for any  $0 \leq \beta \leq 1$ . The method of proof is different from the one presented in [40]. It is based on the approach presented in [17] where it was shown that the classical Dirichlet-Neumann loosely-coupled scheme is unconditionally unstable. The result in [17] was proved on the simplest FSI problem which still retains all the main features responsible for the stability issues associated with the classical loosely coupled schemes. The present manuscript considers the same test problem for which it is shown that the kinematically-coupled  $\beta$ -scheme is unconditionally stable for all  $0 \leq \beta \leq 1$ . The theoretical results are confirmed by numerical simulations which were used to solve a fully nonlinear benchmark problem in FSI in hemodynamics, originally presented in [30] and used for testing of various numerical schemes [5, 42, 3, 46, 33]. The hemodynamics and structure parameters in this benchmark problem fall into the critical regime for which the classical loosely-coupled Dirichlet-Neumann schemes are unstable. Our results show that the kinematically-coupled  $\beta$ -

scheme is stable for those parameters, as predicted by the theory. We also show that the kinematically-coupled  $\beta$ -scheme compares well with the simulations obtained using a monolithic scheme by Badia, Quaini, and Quarteroni [3, 46]. Further numerical results obtained using the kinematically-coupled  $\beta$ -scheme and a comparison with experimental measurements can be found in [12].

We conclude this section by mentioning the most recent generalization of the kinematically-coupled scheme by Fernández et al., called “the incremental displacement-correction scheme” [24, 28, 25]. In [25] the authors prove convergence of this numerical scheme by analyzing a simplified linear model problem. The incremental displacement-correction scheme treats the structure displacement explicitly in the fluid sub-step and then corrects it in the structure sub-step. This scheme can also be viewed as a kinematic perturbation of a semi-implicit scheme. This observation was crucial for proving convergence of the scheme [25]. A different approach, however, needs to be used to prove stability of the kinematically coupled  $\beta$ -scheme due to its particular splitting of the normal stress. This gives rise to the various difficulties in estimating the pressure terms which cannot be handled by using the classical methods presented in [25].

Therefore, the present manuscript provides an original look at the study of stability of the kinematically coupled  $\beta$ -scheme. The method of proof is different from those used in [25, 40]. The results of this manuscript provide the information about the stability of the kinematically coupled  $\beta$ -scheme and its relation to the added mass effect which is not captured by the results in [25, 40]. This is achieved by an “explicit calculation” of the solution to the simplified FSI problem considered here. The main contribution of this work is in explicitly showing how the implicit enforcement of the kinematic coupling condition and the inclusion of the structure inertia into the fluid sub-problem avoid the presence of the added mass effect in the kinematically-coupled  $\beta$ -scheme.

The manuscript is organized as follows. We begin by a description of the kinematically-coupled  $\beta$ -scheme for a full FSI problem in which the structure is modeled by a cylindrical, linearly viscoelastic membrane shell model, also known as the 1D generalized string model. See Section 2. Then, a simplified FSI problem is introduced, and the corresponding application of the kinematically coupled  $\beta$ -scheme is presented, see Section 3. An analysis showing the reasons why the kinematically coupled  $\beta$ -scheme does not suffer from the added-mass effect and is unconditionally stable for any  $0 \leq \beta \leq 1$ , is

presented in Section 4. Numerical results are presented in Section 5 where a fully nonlinear FSI benchmark problem in hemodynamics is considered. Stability of the scheme is shown for the parameter values well within the range of instability of Dirichlet-Neumann schemes. A remark discussing a comparison with the classical Dirichlet-Neumann loosely coupled scheme, and a discussion related to the “added mass effect” are presented in Section 6.

## 2. Problem definition for a fully nonlinear FSI problem

We consider the flow of an incompressible, viscous fluid in a channel of radius  $R$  and length  $L$ , see Figure 1. To fix ideas we will be assuming that the channel is a subset of  $\mathbb{R}^2$ , although none of the ideas related to the definition of the kinematically coupled  $\beta$ -scheme depend on the dimension of the problem. The channel reference domain is denoted by  $\Omega = (0, L) \times (-R, R)$  and the lateral boundary by

$$\Gamma = \{(z, r) \in \mathbb{R}^2 \mid 0 < z < L, r = \pm R\}.$$

The lateral boundary of the channel is assumed to be deformable, with a

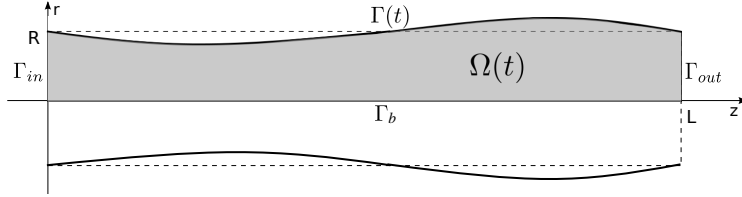


Figure 1: Deformed domain  $\Omega(t)$ .

negligible longitudinal displacement. Without loss of generality, we consider only the upper half of the fluid domain with a symmetry boundary condition at the bottom boundary  $r = 0$ . The fluid domain which depends on time is not known *a priori*. Denote by

$$\Omega(t) = \{(z, r) \in \mathbb{R}^2 : z \in (0, L), r \in (0, R + \eta(z, t))\}$$

the fluid domain at time  $t$ , and the lateral (top) boundary by

$$\Gamma(t) = \{(z, r) \in \mathbb{R}^2 : r = R + \eta(z, t), z \in (0, L)\},$$

where  $\eta$  denotes the vertical (radial) displacement of the lateral boundary. Furthermore, let  $\Gamma_b = (0, L) \times \{0\}$  denote the bottom portion of the boundary,

while  $\Gamma_{in} = \{0\} \times (0, R)$ ,  $\Gamma_{out} = \{L\} \times (0, R)$  denote the inlet and outlet parts, respectively.

We consider the flow of an incompressible, viscous fluid driven by the inlet and outlet pressure data  $p_{in/out}(t)$ , with the fluid velocity on  $\Gamma(t)$  given by  $w\mathbf{e}_r$ , and the symmetry boundary condition at the bottom part of the boundary. Thus, the **fluid problem** reads: Find the fluid velocity  $\mathbf{u} = (u_z(z, r, t), u_r(z, r, t))$  and pressure  $p = p(z, r, t)$  such that

$$\left\{ \begin{array}{ll} \rho_f \left( \frac{\partial \mathbf{u}}{\partial t} + (\mathbf{u} \cdot \nabla) \mathbf{u} \right) = \nabla \cdot \boldsymbol{\sigma} & \text{in } \Omega(t), \ t \in (0, T), \\ \nabla \cdot \mathbf{u} = 0 & \text{in } \Omega(t), \\ u_r = 0, \frac{\partial u_z}{\partial r} = 0 & \text{on } \Gamma_b \times (0, T), \\ \boldsymbol{\sigma} \mathbf{n} = -p_{in/out}(t) & \text{on } \Gamma_{in/out} \times (0, T), \\ \mathbf{u} = w\mathbf{e}_r & \text{on } \Gamma(t), \ t \in (0, T), \end{array} \right. \quad (1)$$

where  $\rho_f$  is the fluid density, and  $\boldsymbol{\sigma}$  is the fluid stress tensor. For a Newtonian fluid the stress tensor is given by  $\boldsymbol{\sigma} = -p\mathbf{I} + 2\mu\mathbf{D}(\mathbf{u})$ , where  $\mu$  is the fluid viscosity and  $\mathbf{D}(\mathbf{u}) = (\nabla \mathbf{u} + (\nabla \mathbf{u})^T)/2$  is the rate-of-strain tensor.

The **structure problem** is defined by solving an elastodynamics problem for a cylindrical linearly viscoelastic membrane shell, also known as a 1D generalized string model [48], capturing only vertical (radial) displacement  $\eta = \eta(z, t)$  from the reference configuration:

$$\rho_s h \frac{\partial^2 \eta}{\partial t^2} + C_0 \eta - C_1 \frac{\partial^2 \eta}{\partial z^2} + D_0 \frac{\partial \eta}{\partial t} - D_1 \frac{\partial^3 \eta}{\partial t \partial z^2} = f, \quad (2)$$

with the boundary conditions  $\eta(0) = \eta(L) = 0$ , and the initial condition given by zero initial displacement and zero initial structure velocity. The coefficients  $\rho_s$  and  $h$  are the structure density and thickness, respectively, while the constants  $C_i, D_i > 0, i = 1, 2$ , are the elastic and viscoelastic structural coefficients [16, 48].

The **coupling** between the fluid and the structure is defined by the kinematic and dynamics lateral boundary conditions, respectively:

$$\begin{aligned} \left( \frac{\partial \eta}{\partial t}(z, t), 0 \right) &= \mathbf{u}(z, R + \eta(z, t), t), \\ f(z, t) &= -J(z, t)(\boldsymbol{\sigma} \mathbf{n})(z, R + \eta(z, t), t) \cdot \mathbf{e}_r, \end{aligned} \quad (3)$$

where  $J(z, t) = -\sqrt{1 + \left( \frac{\partial \eta}{\partial z}(z, t) \right)^2}$  denotes the Jacobian of the transformation from the Eulerian framework used to describe the fluid equations, to the

Lagrangian coordinates used in the structure equations. Here  $f$  in (3) is defined by the left hand-side of (2). The kinematic lateral boundary condition describes continuity of velocities at the fluid-structure interface (the no-slip condition), while the dynamic lateral boundary condition describes the balance of contact forces at the fluid-structure interface: the rate of change of the structure momentum is a result of the balance of all the forces acting at  $\Gamma(t)$ .

### 2.1. The kinematically coupled $\beta$ -scheme

To solve this problem numerically, we consider the kinematically coupled  $\beta$ -scheme, introduced in [11]. This scheme is based on the time-discretization via operator splitting known as the Lie splitting (see e.g., [32, 11]). To perform the Lie splitting, problem (1)-(3) must first be written in the form:  $\partial U / \partial t = AU, t \in (0, T)$ . To do this, we utilize the kinematic lateral boundary condition and express the time-derivative of  $\eta$  as the trace of the fluid velocity on  $\Gamma$ ,  $\mathbf{u}|_{\Gamma} \cdot \mathbf{e}_r$ . The resulting system in first-order form is given by the following:

**Problem 2.1.** Find  $(\mathbf{u}, p, \eta)$  such that

$$\left\{ \begin{array}{llll} \rho_f \left( \frac{\partial \mathbf{u}}{\partial t} + (\mathbf{u} \cdot \nabla) \mathbf{u} \right) & = & \nabla \cdot \boldsymbol{\sigma} & \text{in } \Omega(t), \ t \in (0, T), \\ \nabla \cdot \mathbf{u} & = & 0 & \text{in } \Omega(t), \\ u_r = 0, \ \frac{\partial u_z}{\partial r} = 0 & & & \text{on } \Gamma_b \times (0, T), \\ \boldsymbol{\sigma} \mathbf{n} & = & -p_{in/out}(t) & \text{on } \Gamma_{in/out} \times (0, T), \\ \mathbf{u} & = & \frac{\partial \eta}{\partial t} \mathbf{e}_r & \text{on } \Gamma(t), \ t \in (0, T), \\ \rho_s h \frac{\partial \mathbf{u}}{\partial t} \Big|_{\Gamma} \cdot \mathbf{e}_r + C_0 \eta - C_1 \frac{\partial^2 \eta}{\partial z^2} & & & \\ + D_0 \mathbf{u}|_{\Gamma} \cdot \mathbf{e}_r - D_1 \frac{\partial^2 (\mathbf{u}|_{\Gamma})}{\partial z^2} \cdot \mathbf{e}_r & = & -J \boldsymbol{\sigma} \mathbf{n} \cdot \mathbf{e}_r & \text{on } \Gamma \times (0, T). \end{array} \right.$$

To deal with the motion of the fluid domain an Arbitrary Lagrangian-Eulerian (ALE) approach is used [36, 21, 42]. We introduce a family of (arbitrary, invertible, smooth) mappings  $\mathcal{A}_t$  defined on the reference domain  $\Omega$  such that, for each  $t \in [0, T]$ ,  $\mathcal{A}_t$  maps the reference domain  $\Omega$  onto the current domain



$\Omega(t)$ . Now, ALE time-derivative of function  $f$  defined on  $\Omega(t) \times (0, T)$  is given by

$$\left. \frac{\partial f}{\partial t} \right|_{\hat{\mathbf{x}}} = \frac{\partial f}{\partial t} + \mathbf{w} \cdot \nabla f, \quad (4)$$

where  $\mathbf{w}$  denotes the domain velocity given by

$$\mathbf{w}(z, r, t) = \frac{\partial \mathcal{A}_t}{\partial t}(\hat{z}, \hat{r}), \text{ where } (\hat{z}, \hat{r}) = \mathcal{A}_t^{-1}(z, r). \quad (5)$$

Problem (1)-(3) can now be written in the following first-order ALE form (for more details please see [11]):

**Problem 2.2.** Find  $(\mathbf{u}, p, \eta)$  such that

$$\left\{ \begin{array}{lll} \rho_f \left( \left. \frac{\partial \mathbf{u}}{\partial t} \right|_{\hat{\mathbf{x}}} + ((\mathbf{u} - \mathbf{w}) \cdot \nabla) \mathbf{u} \right) & = & \nabla \cdot \boldsymbol{\sigma} \quad \text{in } \Omega(t), \ t \in (0, T), \\ \nabla \cdot \mathbf{u} & = & 0 \quad \text{in } \Omega(t), \\ u_r = 0, \quad \frac{\partial u_z}{\partial r} = 0 & & \text{on } \Gamma_b \times (0, T), \\ \boldsymbol{\sigma} \mathbf{n} & = & -p_{in/out}(t) \quad \text{on } \Gamma_{in/out} \times (0, T), \\ \mathbf{u} & = & \frac{\partial \eta}{\partial t} \mathbf{e}_r \quad \text{on } \Gamma(t), \ t \in (0, T), \\ \rho_s h \frac{\partial(\mathbf{u}|_{\Gamma})}{\partial t} \cdot \mathbf{e}_r + C_0 \eta - C_1 \frac{\partial^2 \eta}{\partial z^2} & & \\ + D_0 \mathbf{u}|_{\Gamma} \cdot \mathbf{e}_r - D_1 \frac{\partial^2(\mathbf{u}|_{\Gamma})}{\partial z^2} \cdot \mathbf{e}_r & = & -J \boldsymbol{\sigma} \mathbf{n} \cdot \mathbf{e}_r \quad \text{on } \Gamma \times (0, T). \end{array} \right.$$

The strategy of the kinematically coupled scheme is to split this problem into a fluid sub-problem and a structure sub-problem in such a way that the inertia of the thin structure is coupled with the fluid sub-problem via a ‘‘Robin-type’’ boundary condition on  $\Gamma(t)$ . When the structure is viscoelastic, the structural viscosity can be treated together with the structure inertia as a part of the same boundary condition (i.e., all the terms in the structure equation involving the trace of fluid velocity on  $\Gamma$  can be used as a boundary condition for the fluid sub-problem). The elastodynamics of the structure problem is solved separately in the structure sub-problem.

Additionally, in the  $\beta$ -scheme the fluid stress is split into two parts:

$$\boldsymbol{\sigma} \mathbf{n} = \underbrace{\boldsymbol{\sigma} \mathbf{n} + \beta p \mathbf{n}}_{(I)} - \underbrace{\beta p \mathbf{n}}_{(II)}, \quad \beta \in [0, 1],$$

where the case  $\beta = 0$  corresponds to the classical kinematically coupled scheme introduced in [33]. Part I of the fluid stress is used in the fluid sub-problem, while Part II of the fluid stress (the  $\beta$ -fraction of the pressure) is used to load the structure in the elastodynamics sub-problem. Thus, the dynamic coupling condition

$$\begin{aligned} \rho_s h \frac{\partial(\mathbf{u}|_\Gamma)}{\partial t} \cdot \mathbf{e}_r &= -C_0 \eta + C_1 \frac{\partial^2 \eta}{\partial z^2} + \left( D_0 \mathbf{u}|_\Gamma - D_1 \frac{\partial^2(\mathbf{u}|_\Gamma)}{\partial z^2} + J \boldsymbol{\sigma} \mathbf{n} + J \beta p \mathbf{n} \right) \cdot \mathbf{e}_r \\ &\quad - J \beta p \mathbf{n} \cdot \mathbf{e}_r \end{aligned}$$

is split into the fluid part

$$\text{PART 1 : } \rho_s h \frac{\partial(\mathbf{u}|_\Gamma)}{\partial t} \cdot \mathbf{e}_r = -D_0 \mathbf{u}|_\Gamma \cdot \mathbf{e}_r + D_1 \frac{\partial^2(\mathbf{u}|_\Gamma)}{\partial z^2} \cdot \mathbf{e}_r + J \boldsymbol{\sigma} \mathbf{n} \cdot \mathbf{e}_r + J \beta p \mathbf{n} \cdot \mathbf{e}_r,$$

and the structure part

$$\text{PART 2 : } \rho_s h \frac{\partial(\mathbf{u}|_\Gamma)}{\partial t} \cdot \mathbf{e}_r = -C_0 \eta + C_1 \frac{\partial^2 \eta}{\partial z^2} - J \beta p \mathbf{n}, \text{ with } \rho_s h \frac{\partial(\mathbf{u}|_\Gamma)}{\partial t} \cdot \mathbf{e}_r = \rho_s h \frac{\partial^2 \eta}{\partial t^2}.$$

The scheme is then defined by the following.

### The fluid sub-problem:

**Step 1.** The Stokes problem is solved on a fixed fluid domain determined from the previous time step. The boundary condition at lateral boundary is given by PART 1 of the dynamic boundary condition, with  $\beta p \mathbf{n}$  given explicitly from the previous time step. The displacement of the structure stays intact. The problem reads:

Given  $p^n, \eta^n$  from the previous time step, find  $\mathbf{u}, p, \eta$  such that for  $t \in (t^n, t^{n+1})$ :

$$\left\{ \begin{array}{l} \rho_f \frac{\partial \mathbf{u}}{\partial t} \Big|_{\hat{x}} = \nabla \cdot \boldsymbol{\sigma}, \quad \nabla \cdot \mathbf{u} = 0 \quad \text{in } \Omega(t^n) \\ \rho_s h \frac{\partial \mathbf{u}}{\partial t} \Big|_\Gamma \cdot \mathbf{e}_r + D_0 \mathbf{u}|_\Gamma \cdot \mathbf{e}_r - D_1 \frac{\partial^2 \mathbf{u}}{\partial z^2} \Big|_\Gamma \cdot \mathbf{e}_r + \sqrt{1 + \left( \frac{\partial \eta^n}{\partial z} \right)^2} (\boldsymbol{\sigma} \mathbf{n}) \cdot \mathbf{e}_r \\ = -\beta \sqrt{1 + \left( \frac{\partial \eta^n}{\partial z} \right)^2} p^n \mathbf{n} \cdot \mathbf{e}_r \quad \text{on } (0, L), \\ \mathbf{u} \cdot \mathbf{e}_z = 0 \quad \text{on } (0, L), \\ \frac{\partial \eta}{\partial t} = 0 \quad \text{in } (0, L), \end{array} \right.$$

with the following boundary conditions:

$$\frac{\partial u_z}{\partial r}(z, 0, t) = u_r(z, 0, t) = 0 \quad \text{on } \Gamma_b, \quad u_z = 0 \quad \text{on } \Gamma(t^n)$$

$$\mathbf{u}(0, R, t) = \mathbf{u}(L, R, t) = 0,$$

$$\boldsymbol{\sigma} \mathbf{n}|_{in} = -p_{in}(t) \mathbf{n}|_{in} \quad \text{on } \Gamma_{in}, \quad \boldsymbol{\sigma} \mathbf{n}|_{out} = -p_{out}(t) \mathbf{n}|_{out} \quad \text{on } \Gamma_{out},$$

and initial conditions

$$\mathbf{u}(t^n) = \mathbf{u}^n, \quad \eta(t^n) = \eta^n.$$

Then set  $\mathbf{u}^{n+1/3} = \mathbf{u}(t^{n+1})$ ,  $\eta^{n+1/3} = \eta(t^{n+1})$ ,  $p^{n+1} = p(t^{n+1})$ .

**The advection problem:**

**Step 2.** Solve the fluid and ALE advection sub-problem defined on a fixed domain  $\Omega(t^n)$ , with the ALE velocity  $\mathbf{w}^{n+1/3}$  defined by (5) based on the domain  $\Omega(t^n)$  and the corresponding ALE mapping. The problem reads:  
Find  $\mathbf{u}$  and  $\eta$  such that for  $t \in (t^n, t^{n+1})$

$$\begin{cases} \frac{\partial \mathbf{u}}{\partial t}|_{\hat{x}} + (\mathbf{u}^{n+1/3} - \mathbf{w}^{n+1/3}) \cdot \nabla \mathbf{u} = 0, & \text{in } \Omega(t^n) \\ \frac{\partial \eta}{\partial t} = 0 & \text{on } (0, L), \\ \rho_s h_s \frac{\partial \mathbf{u}}{\partial t}|_{\Gamma} = 0, & \text{on } (0, L), \end{cases}$$

with the following boundary conditions:

$$\mathbf{u} = \mathbf{u}^{n+1/3} \quad \text{on } \Gamma_-^{n+1/3}, \quad \text{where}$$

$$\Gamma_-^{n+1/3} = \{\mathbf{x} \in \mathbb{R}^2 | \mathbf{x} \in \partial\Omega(t^n), (\mathbf{u}^{n+1/3} - \mathbf{w}^{n+1/3}) \cdot \mathbf{n} < 0\},$$

and the initial conditions

$$\mathbf{u}(t^n) = \mathbf{u}^{n+1/3}, \quad \eta(t^n) = \eta^{n+1/3}.$$

Then set  $\mathbf{u}^{n+2/3} = \mathbf{u}(t^{n+1})$ ,  $\eta^{n+2/3} = \eta(t^{n+1})$ .

**The structure (elastodynamics) sub-problem:**

**Step 3.** Step 3 involves solving the elastodynamics problem for the location of the deformable boundary by involving the elastic part of the structure which is loaded by Part II of the normal fluid stress. Additionally, the fluid and structure communicate via the kinematic lateral boundary condition which gives the velocity of the structure in terms of the trace of the fluid velocity, taken initially to be the value from the previous step. The problem reads:

Find  $\mathbf{u}$  and  $\eta$ , with  $p^{n+1}$  computed in Step 1 and  $\eta^n$  obtained at the previous time step, such that for  $t \in (t^n, t^{n+1})$

$$\left\{ \begin{array}{l} \frac{\partial \mathbf{u}}{\partial t} \big|_{\hat{x}} = 0, \quad \text{in } \Omega(t^n) \\ \frac{\partial \eta}{\partial t} = \mathbf{u}|_{\Gamma(t)} \cdot \mathbf{e}_r \quad \text{on } (0, L), \\ \rho_s h \frac{\partial \mathbf{u}}{\partial t} \big|_{\Gamma} \cdot \mathbf{e}_r + C_0 \eta - C_1 \frac{\partial^2 \eta}{\partial z^2} = \beta \sqrt{1 + \left( \frac{\partial \eta^n}{\partial z} \right)^2} p^{n+1} \mathbf{n} \cdot \mathbf{e}_r \quad \text{on } (0, L), \end{array} \right.$$

with the boundary conditions:

$$\eta|_{z=0,L} = 0,$$

and the initial conditions:

$$\mathbf{u}(t^n) = \mathbf{u}^{n+2/3}, \quad \eta(t^n) = \eta^{n+2/3}.$$

Then set  $\mathbf{u}^{n+1} = \mathbf{u}(t^{n+1})$ ,  $\eta^{n+1} = \eta(t^{n+1})$ .

Do  $t^n = t^{n+1}$  and return to Step 1.

A block-diagram showing the main steps of the scheme is given in Figure 2.1. More details about the scheme can be found in [11].

### 3. The simplified test problem

We show that the kinematically coupled  $\beta$ -scheme is unconditionally stable when applied to a simplified problem, introduced in [17] as the simplest problem which captures the main features related to the instabilities in classical loosely-coupled schemes caused by the “added mass effect”. The simplified problem consists of solving the time-dependent Stokes equations for

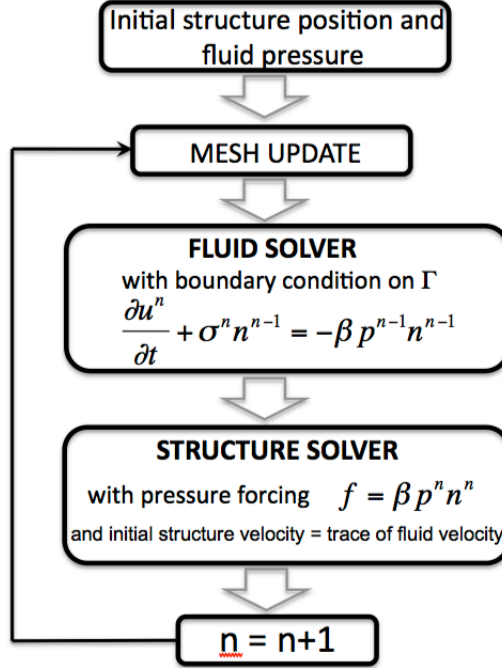


Figure 2: A block diagram showing the main steps of the kinematically coupled  $\beta$ -scheme.

an incompressible, inviscid fluid in a 2D channel with deformable walls, and with the elastodynamics equations given by the 1D generalized string model. Moreover, it is assumed that the displacement of the deformable wall is small enough so that it can be neglected in the fluid flow problem. In this case the geometry of the fluid domain is fixed while the small deformation of the boundary is calculated using the elastodynamics equations which are coupled with the fluid flow through the kinematic and dynamic coupling conditions. Thus, the problem is defined on the reference fluid domain  $\Omega$  with the lateral boundary  $\Gamma$ .

We will be assuming that the inlet and outlet pressure data, which are functions of time, are uniformly bounded. This is a reasonable assumption for the blood flow application, since the pressure is typically a periodic function of time, with a bounded amplitude.

The **fluid problem** reads: Find the fluid velocity  $\mathbf{u} = \mathbf{u}(z, r, t)$  and

pressure  $p = p(z, r, t)$  such that

$$\left\{ \begin{array}{ll} \rho_f \frac{\partial \mathbf{u}}{\partial t} + \nabla p = 0 & \text{in } \Omega \times (0, T), \\ \nabla \cdot \mathbf{u} = 0 & \text{in } \Omega \times (0, T), \\ \mathbf{u} \cdot \mathbf{n} = 0 & \text{on } \Gamma_b \times (0, T), \\ p = p_{in/out}(t) & \text{on } \Gamma_{in/out} \times (0, T), \\ \mathbf{u} \cdot \mathbf{e}_r = w & \text{on } \Gamma \times (0, T), \end{array} \right. \quad (6)$$

with the initial velocity and pressure equal to zero.

The **structure problem** is defined by solving for  $\eta = \eta(z, t)$  the 1D generalized string model:

$$\rho_s h \frac{\partial^2 \eta}{\partial t^2} + C_0 \eta - C_1 \frac{\partial^2 \eta}{\partial z^2} = f, \quad (7)$$

with boundary conditions  $\eta(0) = \eta(L) = 0$ , and initial conditions given by the zero initial displacement and zero initial structure velocity.

**Remark 3.1.** *Notice that the simplified problem does not have the viscoelastic terms. The addition of the viscoelastic terms only contributes to the stability of the scheme. For more details about the analysis of the fully nonlinear FSI problem with and without the viscoelastic terms see [40].*

The **coupling** between the fluid and structure is defined by the kinematic and dynamic lateral boundary conditions, which, in this simplified problem, read:

$$\begin{aligned} f &= p|_{\Gamma}, \\ \left( \frac{\partial \eta}{\partial t}, 0 \right) &= \mathbf{u}|_{\Gamma}. \end{aligned} \quad (8)$$

The coupled fluid-structure interaction problem can be written as follows:

**Problem 3.1.**

$$\left\{ \begin{array}{ll} \rho_f \frac{\partial \mathbf{u}}{\partial t} + \nabla p = 0 & \text{in } \Omega \times (0, T), \\ \nabla \cdot \mathbf{u} = 0 & \text{in } \Omega \times (0, T), \\ \mathbf{u} \cdot \mathbf{n} = 0 & \text{on } \Gamma_b \times (0, T), \\ p = p_{in/out}(t) & \text{on } \Gamma_{in/out} \times (0, T), \\ \mathbf{u} \cdot \mathbf{e}_r = \frac{\partial \eta}{\partial t} & \text{on } \Gamma \times (0, T), \\ p = \rho_s h \frac{\partial^2 \eta}{\partial t^2} + C_0 \eta - C_1 \frac{\partial^2 \eta}{\partial z^2} & \text{on } \Gamma \times (0, T). \end{array} \right. \quad (9)$$

To perform the Lie splitting, this system is written as a first-order system by using the kinematic coupling condition to obtain:

$$\left\{ \begin{array}{ll} \rho_f \frac{\partial \mathbf{u}}{\partial t} + \nabla p = 0 & \text{in } \Omega \times (0, T), \\ \nabla \cdot \mathbf{u} = 0 & \text{in } \Omega \times (0, T), \\ \mathbf{u} \cdot \mathbf{n} = 0 & \text{on } \Gamma_b \times (0, T), \\ p = p_{in/out}(t) & \text{on } \Gamma_{in/out} \times (0, T), \\ \mathbf{u} \cdot \mathbf{e}_r = \frac{\partial \eta}{\partial t} & \text{on } \Gamma \times (0, T), \\ p = \rho_s h \frac{\partial \mathbf{u}}{\partial t} \Big|_{\Gamma} \cdot \mathbf{e}_r + C_0 \eta - C_1 \frac{\partial^2 \eta}{\partial z^2} & \text{on } \Gamma \times (0, T). \end{array} \right. \quad (10)$$

As before, this point is crucial in order to perform the splitting which gives rise to a stable scheme. Namely, in the fluid sub-problem, which we write next, the structure inertia will be taken into account implicitly in the boundary condition on  $\Gamma$ , which is a crucial ingredient for the stability of the  $\beta$ -scheme.

Before we write the main splitting steps we also notice that the fluid stress, which in this simplified example is only the pressure, will be split into two parts: Part I which is given by  $p - \beta p$ , and Part 2 which is given by  $\beta p$  so that  $p = (p - \beta p) + \beta p$  = Part 1 + Part 2.

Thus, the main steps of the Lie splitting for the simplified FSI problem (10) are:

### The fluid sub-problem:

**Step 1.** The Stokes problem is solved on a fixed fluid domain, with a boundary condition which couples the structure inertia with the Part I of the fluid stress. Here, the portion  $\beta p$  of the stress is taken explicitly, while the rest is taken implicitly. The displacement of the structure stays intact. The problem reads: *Given  $p^n$  from the previous time step, find  $\mathbf{u}, \eta$  and  $p$  such that for  $t \in (t^n, t^{n+1})$ :*

$$\left\{ \begin{array}{ll} \rho_f \frac{\partial \mathbf{u}}{\partial t} + \nabla p = 0 & \text{in } \Omega, \\ \nabla \cdot \mathbf{u} = 0 & \text{in } \Omega, \\ \mathbf{u} \cdot \mathbf{n} = 0 & \text{on } \Gamma_b, \\ p = p_{in/out}(t) & \text{on } \Gamma_{in/out}, \\ p - \beta p^n = \rho_s h \frac{\partial \mathbf{u}}{\partial t} \Big|_{\Gamma} \cdot \mathbf{e}_r & \text{on } \Gamma. \end{array} \right. \quad (11)$$

The structure displacement stays intact, namely

$$\frac{\partial \eta}{\partial t} = 0 \quad \text{on} \quad \Gamma. \quad (12)$$

The initial conditions are taken from the previous time step. Then set

$$\mathbf{u}^{n+1/2} = \mathbf{u}(t^{n+1}), \mathbf{u}|_{\Gamma}^{n+1/2} = \mathbf{u}|_{\Gamma}(t^{n+1}), p^{n+1} = p(t^{n+1}). \quad (13)$$

### The structure sub-problem:

**Step 2.** The structure problem is solved with the pressure load  $\beta p^{n+1}$  just calculated from the fluid sub-problem: Find  $\mathbf{u}$  and  $\eta$  such that for  $t \in (t^n, t^{n+1})$  the following holds:

$$\begin{cases} \rho_s h \frac{\partial \mathbf{u}}{\partial t} \Big|_{\Gamma} \cdot \mathbf{e}_r + C_0 \eta - C_1 \frac{\partial^2 \eta}{\partial z^2} = \beta p^{n+1} \Big|_{\Gamma} & \text{on } (0, L), \\ \frac{\partial \eta}{\partial t}(z, t) = \mathbf{u}|_{\Gamma} \cdot \mathbf{e}_r & \text{on } (0, L) \end{cases}$$

The fluid velocity in  $\Omega$  remains intact, namely:

$$\frac{\partial \mathbf{u}}{\partial t} = 0 \quad \text{in } \Omega.$$

The initial data correspond to the solution of the problem in Step 1 evaluated at  $t^{n+1}$ . Then set

$$\mathbf{u}^{n+1} = \mathbf{u}(t^{n+1}), \mathbf{u}|_{\Gamma}^{n+1} = \mathbf{u}|_{\Gamma}(t^{n+1}), \eta^{n+1} = \eta(t^{n+1}). \quad (14)$$

### The pressure formulation:

In this simplified model, the problem in Step 1 can be entirely formulated in terms of the pressure and the normal trace of the fluid velocity on  $\Gamma$ . Namely, by taking the divergence free condition in the differentiated first (momentum) equation, the problem can be written in terms of the Laplace operator for the pressure. Similarly, we can re-write the boundary conditions on  $\Gamma$  in terms of the pressure and the normal trace of the velocity on  $\Gamma$ .

To simplify notation we will be using  $\mathbf{n}$  to denote the normal,  $\mathbf{e}_r$ , on  $\Gamma$ , and  $u_r|_{\Gamma}$  to denote the normal trace of the fluid velocity on  $\Gamma$ :

$$\mathbf{n} := \mathbf{e}_r \quad \text{on } \Gamma \quad \text{and} \quad u_r|_{\Gamma} := \mathbf{u}|_{\Gamma} \cdot \mathbf{e}_r.$$



**The fluid sub-problem in terms of  $p$  and  $u_r|_\Gamma$**

**Step 1'.** Find  $p$  and  $u_r|_\Gamma$  such that for  $t \in (t^n, t^{n+1})$ :

$$\left\{ \begin{array}{lll} -\Delta p & = & 0, \quad \text{in } \Omega, \\ p & = & p_{in/out}(t) \quad \text{on } \Gamma_{in/out}, \\ \frac{\partial p}{\partial \mathbf{n}} & = & 0 \quad \text{on } \Gamma_b, \\ p + \frac{\rho_s h}{\rho_f} \frac{\partial p}{\partial \mathbf{n}} & = & \beta p^n \quad \text{on } \Gamma, \\ \hline \frac{\partial u_r|_\Gamma}{\partial t} & = & -\frac{1}{\rho_f} \frac{\partial p|_\Gamma}{\partial \mathbf{n}} \quad \text{on } \Gamma, \end{array} \right.$$

The first four equations in Step 1', supplemented with the initial data for the pressure determine a time-dependent Robin problem for the pressure. The time-dependence enters through the inlet and outlet pressure data, which are functions of time. Notice that this problem already incorporates a portion of the coupling of the underlying FSI problem. This problem has a unique solution in the space  $C(0, \infty; H^1(\Omega))$  provided that the data  $p_{in/out} \in C(0, \infty; H^{1/2}(\Gamma_{in/out}))$ , and  $p^n \in C(0, \infty; H^{-1/2}(\Gamma))$ .

One can also show (see e.g., [17]) that the problem for the structure, defined in Step 2, has a unique solution  $\eta \in C((0, \infty); H_0^1(0, L))$  provided that the initial data are such that  $\eta|_{t=0} \in H_0^1(0, L)$ , and  $\partial\eta/\partial t|_{t=0} \in H_0^1(0, L)$ , with  $p^{n+1}|_\Gamma \in C(0, \infty; H^{1/2}(\Gamma))$ .

To simplify notation, as in [17], we introduce a linear, symmetric, positive definite operator  $\mathcal{L}$  defined by the elasticity tensor associated with the structure problem. Namely, for  $\eta, \xi \in H_0^1(0, L)$ , we define

$$\langle \mathcal{L}\eta, \xi \rangle := a_S(\eta, \xi), \quad (15)$$

where  $a_S(\eta, \xi)$  is the inner product on  $H^1(0, L)$  defined by

$$a_S(\eta, \xi) := \int_0^L C_0 \eta \xi dx + \int_0^L C_1 \frac{\partial \eta}{\partial x} \frac{\partial \xi}{\partial x} dx, \quad \forall \eta, \xi \in H^1(0, L).$$

With this notation, the structure equation in Step 2 can be written as

$$\rho_s h \frac{\partial^2 \eta}{\partial t^2} + \mathcal{L}\eta = \beta p|_\Gamma.$$

Operator  $\mathcal{L}$  can be extended to the full structure operator defining the Koiter shell model, described in [16].

We now summarize the main steps of the splitting scheme. With a slight abuse of notation, we emphasize the discretized form of the Lie splitting, defining our kinematically coupled  $\beta$ -scheme:

**Step 1.** Given  $u_r^n|_\Gamma$ ,  $p^n, \eta^n$ , find  $p^{n+1/2}$ ,  $u_r^{n+1/2}|_\Gamma$ ,  $\eta^{n+1/2}$ , such that for  $t \in (t^n, t^{n+1})$ :

$$\left\{ \begin{array}{lll} -\Delta p^{n+1/2} & = & 0, \quad \text{in } \Omega, \\ p^{n+1/2} & = & p_{in/out}(t) \quad \text{on } \Gamma_{in/out}, \\ \frac{\partial p^{n+1/2}}{\partial \mathbf{n}} & = & 0 \quad \text{on } \Gamma_b, \\ p^{n+1/2} + \frac{\rho_s h}{\rho_f} \frac{\partial p^{n+1/2}}{\partial \mathbf{n}} & = & \beta p^n \quad \text{on } \Gamma, \\ \hline \frac{\partial(u_r^{n+1/2}|_\Gamma)}{\partial t} & = & -\frac{1}{\rho_f} \frac{\partial p^{n+1/2}|_\Gamma}{\partial \mathbf{n}} \quad \text{on } \Gamma, \\ \eta^{n+1/2} & = & \eta^n \quad \text{on } \Gamma. \end{array} \right.$$

with the initial data given by  $u_r^n|_\Gamma$ ,  $p^n, \eta^n$ .

**Step 2.** Given  $p^{n+1/2}$ ,  $u_r^{n+1/2}|_\Gamma$ ,  $\eta^{n+1/2}$  find  $p^{n+1}$ ,  $u_r^{n+1}|_\Gamma$ ,  $\eta^{n+1}$ , such that for  $t \in (t^n, t^{n+1})$ :

$$\left\{ \begin{array}{lll} \rho_s h \frac{\partial^2 \eta^{n+1}}{\partial t^2} + \mathcal{L} \eta^{n+1} & = & \beta p^{n+1/2}|_\Gamma \quad \text{on } \Gamma \\ u_r^{n+1}|_\Gamma & = & \frac{\partial \eta^{n+1}}{\partial t} \quad \text{on } \Gamma \\ p^{n+1} & = & p^{n+1/2} \quad \text{on } \Omega. \end{array} \right.$$

with the initial data given by  $p^{n+1/2}$ ,  $u_r^{n+1/2}|_\Gamma$ ,  $\eta^{n+1/2}$  at  $t^{n+1}$ .

We study the stability of the kinematically coupled  $\beta$ -scheme for this problem next.

#### 4. Stability analysis

To study the stability we introduce an operator  $\mathcal{P} : H^{-1/2}(\Gamma) \rightarrow Q$ , where

$$Q = \{q \in H^1(\Omega) \mid q|_{\Gamma_{in/out}} = 0\}, \quad (16)$$

such that

$$\left\{ \begin{array}{ll} -\Delta \mathcal{P}w &= 0, \text{ in } \Omega, \\ \mathcal{P}w &= 0 \text{ on } \Gamma_{in/out}, \\ \frac{\partial \mathcal{P}w}{\partial \mathbf{n}} &= 0 \text{ on } \Gamma_b, \\ \mathcal{P}w + \frac{\rho_s h}{\rho_f} \frac{\partial \mathcal{P}w}{\partial \mathbf{n}} &= w \text{ on } \Gamma. \end{array} \right. \quad (17)$$

Thus, operator  $\mathcal{P}$  associates to every  $w \in H^{-1/2}(\Gamma)$  the solution of the pressure problem in Step 1', with the homogeneous inlet and outlet data  $p_{in/out} = 0$ .

We are interested in the trace on  $\Gamma$  of this pressure solution. For this purpose, introduce the operator  $\mathcal{S} : H^{-1/2}(\Gamma) \rightarrow H^{1/2}(\Gamma)$  by

$$\mathcal{S}w = \mathcal{P}w|_{\Gamma}. \quad (18)$$

One can prove the following standard results (see [17]):

**Proposition 4.1.** *The operator  $\mathcal{S}$  satisfies the following properties:*

1. *The operator  $\mathcal{S} : H^{-1/2}(\Gamma) \rightarrow H^{1/2}(\Gamma)$  is continuous.*
2. *The operator  $\mathcal{S}$  is compact, self-adjoint, and positive on  $L^2(\Gamma)$ .*

**Proof.** Since this result is quite standard, we just outline the proof. We start by writing the weak formulation of problem (17) which reads: find  $\mathcal{P}w \in Q$  such that

$$\int_{\Omega} \nabla \mathcal{P}w : \nabla \phi + \frac{\rho_f}{\rho_s h} \int_{\Gamma} \mathcal{P}w \phi = \frac{\rho_f}{\rho_s h} \langle w, \phi \rangle, \quad \forall \phi \in Q, \quad (19)$$

where  $\langle w, \phi \rangle$  is a duality pairing between  $H^{-1/2}(\Gamma)$  and  $H^{1/2}(\Gamma)$ . The first assertion (continuity) follows directly from here.

To show the second statement of the proposition, we consider  $w, v \in L^2(\Gamma)$  and notice:

$$\int_{\Gamma} \mathcal{S}wv = \int_{\Gamma} \mathcal{P}wv = \frac{\rho_s h}{\rho_f} \int_{\Omega} \nabla \mathcal{P}v : \nabla \mathcal{P}w + \int_{\Gamma} \mathcal{P}v \mathcal{P}w. \quad (20)$$

Here, the first equality follows from the definition of operator  $\mathcal{S}$ . For the second equality we notice that  $\mathcal{P}w \in Q$  is an admissible test function and, therefore, the second equality is just formula (19) with the test function  $\phi = \mathcal{P}w$ . Now, we consider  $\mathcal{P}$  as an operator on  $L^2(\Gamma)$ , i.e.,  $\mathcal{S} : L^2(\Gamma) \rightarrow L^2(\Gamma)$ .

For every  $w \in L^2(\Gamma)$ , we have  $\mathcal{P}w \in Q$ . Now, the trace theorem implies that  $\mathcal{S}w = \mathcal{P}w|_\Gamma \in H^{1/2}(\Gamma)$  and so we have  $\text{Im}(\mathcal{S}) \subseteq H^{1/2}(\Gamma)$ . Since  $\Gamma$  is a bounded set, embedding  $H^{1/2}(\Gamma) \hookrightarrow L^2(\Gamma)$  is compact, and thus  $\mathcal{S}$  is a compact operator. Formula (20) implies that operator  $\mathcal{S}$  is positive and self-adjoint, which completes the proof.  $\square$

To study the solution of the corresponding non-homogeneous problem with  $p = p_{in/out}(t)$  on  $\Gamma_{in/out}$ , let us introduce an arbitrary continuous extension operator  $E_F : H^{1/2}(\partial\Omega \setminus \Gamma) \rightarrow H^1(\Omega)$  so that  $E_F q|_{\partial\Omega \setminus \Gamma} = q$  and  $\|E_F q\|_{H^1(\Omega)} \leq C \|q\|_{H^{1/2}(\partial\Omega \setminus \Gamma)}$ . Let  $p^* \in C(0, \infty; H^1(\Omega))$  be the solution to

$$\left\{ \begin{array}{ll} -\Delta p^* = \Delta E_F \bar{p}, & \text{in } \Omega, \\ p^* = 0 & \text{on } \Gamma_{in/out}, \\ \frac{\partial p^*}{\partial \mathbf{n}} = -\frac{\partial E_F \bar{p}}{\partial \mathbf{n}} & \text{on } \Gamma_b, \\ p^* + \frac{\rho_s h}{\rho_f} \frac{\partial p^*}{\partial \mathbf{n}} = -\frac{\partial E_F \bar{p}}{\partial \mathbf{n}} & \text{on } \Gamma, \end{array} \right.$$

where  $\bar{p} = p_{in/out}$  on  $\Gamma_{in/out}$ . Now, the solution to the pressure problem in Step 1' is given by

$$p = p^* + E_F \bar{p} + \mathcal{P}(\beta p^n).$$

Let us denote

$$p_{ext} = p^*|_\Gamma + E_F \bar{p}|_\Gamma.$$

Now we can write the trace of the pressure solution in Step 1' on  $\Gamma$  as

$$p|_\Gamma = p_{ext} + \mathcal{S}(\beta p^n). \quad (21)$$

This trace of the pressure is used to load the equation for the structure in Step 2. Thus, the structure problem in Step 2 can now be written as: *Find  $\eta$  such that*

$$\rho_s h \frac{\partial^2 \eta}{\partial t^2} + \mathcal{L}\eta = \beta(p_{ext}^{n+1} + \mathcal{S}(\beta p^n)). \quad (22)$$

One way to discretize this equation in time is to use an implicit marching scheme

$$\rho_s h \frac{\eta^{n+1} - 2\eta^n + \eta^{n-1}}{\Delta t^2} + \mathcal{L}\eta^{n+1} = \beta(p_{ext}^{n+1} + \mathcal{S}(\beta p^n)). \quad (23)$$

This scheme is unconditionally stable (provided that the right hand-side converges).

We chose to discretize equation (22) in time using a  $\theta$ -scheme discussed in [32]:

$$\rho_s h \frac{\eta^{n+1} - 2\eta^n + \eta^{n-1}}{\Delta t^2} + \mathcal{L}(\theta\eta^{n+1} + (1-2\theta)\eta^n + \theta\eta^{n-1}) = \beta(p_{ext}^{n+1} + \mathcal{S}(\beta p^n)). \quad (24)$$

It was shown in [32] that, for a given fixed right hand-side (source term), this scheme is stable for all  $0 \leq \theta \leq 1/2$ . Thus, we have unconditional stability with respect to the arbitrary ratios of the fluid and structure densities, provided that the right hand-side of this equation converges as  $n \rightarrow \infty$ .

A crucial point to observe here is that the right hand-side of this equation, which comes from the pressure loading, is given by an iterative procedure, and can be written entirely in terms of the initial pressure, the external pressure ( $p_{in/out}$ ), and the operator  $\mathcal{S}$  whose maximum eigenvalue, as we shall show below, is always less than 1, for all the choices of  $\rho_f$  and  $\rho_s h$ . Moreover, we will show below that the right hand-side converges, as the number of iterations  $n \rightarrow \infty$  if  $0 \leq \beta \leq 1$ , for all the choices of  $\rho_f$  and  $\rho_s h$ .

To analyze the right hand-side of equation (22), we first study the eigenvalues of the operator  $\mathcal{S}$ . As we shall see below, it is convenient to express the eigenvalues of  $\mathcal{S}$  via the eigenvalues of the “Neumann to Dirichlet” operator  $\mathcal{M}_A : H^{-1/2}(\Gamma) \rightarrow H^{1/2}(\Gamma)$  which is defined to be the trace on  $\Gamma$  of the operator  $\mathcal{R} : H^{-1/2}(\Gamma) \rightarrow Q$ :

$$\mathcal{M}_A w = \mathcal{R}w|_{\Gamma}, \quad (25)$$

where  $\mathcal{R}$  associates to every  $w \in H^{-1/2}(\Gamma)$  the solution  $\mathcal{R}w \in Q$  of the following (pressure) problem:

$$\left\{ \begin{array}{ll} -\Delta \mathcal{R}w &= 0, \quad \text{in } \Omega, \\ \mathcal{R}w &= 0 \quad \text{on } \Gamma_{in/out}, \\ \frac{\partial \mathcal{R}w}{\partial \mathbf{n}} &= 0 \quad \text{on } \Gamma_b, \\ \frac{\partial \mathcal{R}w}{\partial \mathbf{n}} &= w \quad \text{on } \Gamma. \end{array} \right.$$

It can be shown (see [17]) that operator  $\mathcal{M}_A : H^{-1/2}(\Gamma) \rightarrow H^{1/2}(\Gamma)$  is continuous, and that  $\mathcal{M}_A$  is compact, self-adjoint, and positive on  $L^2(\Gamma)$ . Moreover, the eigenvalues  $\mu_i$  of  $\mathcal{M}_A$  are decreasing to zero ( $\mu_i = L/(i\pi \text{th}(i\pi R/L))$ ),  $i =$

1,2,...), with the maximum eigenvalue  $\mu_{max}$  given by

$$\mu_{max} = \mu_1 = \frac{L}{\pi \text{th}\left(\frac{\pi R}{L}\right)}.$$

We will use this knowledge to calculate the eigenvalues of operator  $\mathcal{S}$ . Let  $\mu$  be an eigenvalue of operator  $\mathcal{M}_A$ . Then there exists a vector  $v \neq 0$  such that

$$\mathcal{M}_A v = \mu v.$$

Recall that, by definition of  $\mathcal{M}_A$ ,  $\mathcal{M}_A v = \mathcal{R}v|_\Gamma$  and  $\frac{\partial \mathcal{R}v}{\partial \mathbf{n}} = v$ . Using this, we calculate

$$\mathcal{R}v|_\Gamma + \frac{\rho_s h}{\rho_f} \frac{\partial \mathcal{R}v}{\partial \mathbf{n}}|_\Gamma = \left(\mu + \frac{\rho_s h}{\rho_f}\right)v|_\Gamma.$$

This implies that  $\mathcal{R}v$  also satisfies the following Robin problem:

$$\left\{ \begin{array}{ll} -\Delta \mathcal{R}v &= 0, & \text{in } \Omega, \\ \mathcal{R}v &= 0 & \text{on } \Gamma_{in/out}, \\ \frac{\partial \mathcal{R}v}{\partial \mathbf{n}} &= 0 & \text{on } \Gamma_b, \\ \mathcal{R}v + \frac{\rho_s h}{\rho_f} \frac{\partial \mathcal{R}v}{\partial \mathbf{n}} &= \left(\mu + \frac{\rho_s h}{\rho_f}\right)v & \text{on } \Gamma. \end{array} \right.$$

But this is precisely the problem defined by the operator  $\mathcal{P}$  in (17), with the data on  $\Gamma$  given by  $(\mu + \frac{\rho_s h}{\rho_f})v$ . Thus:

$$\mathcal{R}v = \mathcal{P}\left(\mu + \frac{\rho_s h}{\rho_f}\right)v,$$

and therefore, the traces on  $\Gamma$  satisfy:

$$\mathcal{M}_A v = \mathcal{S}\left(\mu + \frac{\rho_s h}{\rho_f}\right)v = \left(\mu + \frac{\rho_s h}{\rho_f}\right)\mathcal{S}v.$$

Since  $\mathcal{M}_A v = \mu v$  we finally get

$$\mu v = \left(\mu + \frac{\rho_s h}{\rho_f}\right)\mathcal{S}v.$$

Therefore,  $v$  is also an eigenvector for  $\mathcal{S}$ , and the corresponding eigenvalue  $\lambda$  satisfies:

$$\lambda = \frac{\mu}{\mu + \frac{\rho_s h}{\rho_f}}. \quad (26)$$

Thus, we have shown that the eigenvalues  $\lambda_i$  of  $\mathcal{S}$  can be expressed using the eigenvalues  $\mu_i$  of  $\mathcal{M}_A$  as

$$\lambda_i = \frac{\mu_i}{\mu_i + \frac{\rho_s h}{\rho_f}}, i = 1, 2, \dots \quad (27)$$

We now use this information to study the right hand-side of equation (24). Since  $\mathcal{S}$  is compact, there exists an orthonormal basis of  $L^2(\Gamma)$  composed of the eigenvectors  $\{z_j\}$  of  $\mathcal{S}$ . We thus expand the solution  $\eta$  and the external pressure data  $p_{ext}$  and  $p^0$  in this basis:

$$\eta^n = \sum_j (\eta^n)_j z_j, \quad p_{ext}^n = \sum_j (p_{ext}^n)_j z_j, \quad p_0 = \sum_j (p_0)_j z_j.$$

Then, from (24), for each  $j$ , the Fourier coefficients satisfy the following equation:

$$\begin{aligned} \rho_s h \frac{(\eta^{n+1})_j - 2(\eta^n)_j + (\eta^{n-1})_j}{\Delta t^2} + \mathcal{L}(\theta(\eta_r^{n+1})_j + (1 - 2\theta)(\eta^n)_j + \theta(\eta^{n-1})_j) \\ = \beta((p_{ext}^{n+1})_j + \mathcal{S}(\beta(p^n))_j). \end{aligned} \quad (28)$$

The right hand-side of this equation is equal to

$$\begin{aligned} \beta((p_{ext}^{n+1})_j + \mathcal{S}(\beta(p^n))_j) = \\ \beta(p_{ext}^{n+1})_j + \sum_{i=1}^n \beta^{i+1} \lambda_j^i (p_{ext}^{n+1-i})_j + \beta^{n+2} \lambda_j^{n+1} (p_0)_j. \end{aligned}$$

As  $n \rightarrow \infty$ , the series that defines the right hand-side converges if

$$|\beta \lambda_j| < 1.$$

From (27) we see that all  $\lambda_j$  are strictly less than one, which implies that the right hand-side converges if

$$0 \leq \beta \leq 1. \quad (29)$$

We have shown the following result:

**Theorem 4.1.** *The kinematically coupled  $\beta$ -scheme applied to a class of FSI problems represented by the simple benchmark problem (10), is unconditionally stable for each  $\beta$  such that  $0 \leq \beta \leq 1$ .*

## 5. Numerical results

We present two numerical examples that show stability of the kinematically coupled  $\beta$ -scheme for a fully nonlinear FSI problem. The parameter values in the two examples are well within the range for which the classical Dirichlet-Neumann schemes are unstable. Numerical simulations in both cases are performed on a benchmark problem by Formaggia et al. [30] used for testing of several FSI algorithms in hemodynamics applications [5, 42, 3, 46, 33].

It was shown in [17] that the classical loosely coupled, Dirichlet-Neumann scheme is unconditionally unstable if

$$\frac{\rho_s h}{\rho_f \mu_{max}} < 1, \quad (30)$$

where  $\mu_{max}$  is the maximum eigenvalue of the added mass operator given by

$$\mu_{max} = \frac{L}{\pi \tanh\left(\frac{\pi R}{L}\right)}.$$

For the parameters given in Table 1, the value of  $\mu_{max}$  is 7.46, so the critical value for the structure density is  $\rho_s = 74.6 \text{ g/cm}^3$ . Therefore, the classical Dirichlet-Neumann scheme is unconditionally unstable if  $\rho_s < 74.6 \text{ g/cm}^3$ . In Example 1, we take the density of the structure to be 70-times smaller, given by the physiologically relevant value of  $\rho_s = 1.1 \text{ g/cm}^3$ . We compare our results with the results obtained using a monolithic scheme by Badia, Quaini and Quarteroni [3, 46] showing excellent agreement. In Example 2, we choose an even smaller structural density,  $\rho_s = 0.55 \text{ g/cm}^3$ , and show the convergence of our scheme in time, confirming the stability of the kinematically coupled  $\beta$ -scheme even for the fully nonlinear FSI problems.

### The benchmark problem [30]:

The benchmark problem consists of solving the fully nonlinear FSI problem (1)-(3) with the values of the coefficients for the fluid problem given in Table 1, and the values of the structural coefficients given in Table 2.

The flow is driven by the time-dependent pressure data:

$$p_{in}(t) = \begin{cases} \frac{p_{max}}{2} \left[ 1 - \cos\left(\frac{2\pi t}{t_{max}}\right) \right] & \text{if } t \leq t_{max} \\ 0 & \text{if } t > t_{max} \end{cases}, \quad p_{out}(t) = 0 \quad \forall t \in (0, T), \quad (31)$$



Parameters	Values	Parameters	Values
<b>Radius</b> $R$ (cm)	0.5	<b>Length</b> $L$ (cm)	6
<b>Fluid density</b> $\rho_f$ (g/cm <sup>3</sup> )	1	<b>Dyn. viscosity</b> $\mu$ (poise)	0.035
<b>Young's mod.</b> $E$ (dynes/cm <sup>2</sup> )	$0.75 \times 10^6$	<b>Wall thickness</b> $h_s$ (cm)	0.1
<b>Poisson's ratio</b> $\sigma$	0.5		

Table 1: Geometric parameters, and fluid and structural parameters that are used in Examples 1 and 2 presented in this section.

Coefficients	Values	Coefficients	Values
$C_0$	$4 \times 10^5$	$C_1$	$2.5 \times 10^4$
$D_0$	0	$D_1$	0.01

Table 2: The values of the coefficients in (2) used in Examples 1 and 2 below.

where  $p_{max} = 2 \times 10^4$  (dynes/cm<sup>2</sup>) and  $t_{max} = 0.005$  (s). The graph of the inlet pressure data versus time is shown in Figure 3. The inlet and outlet

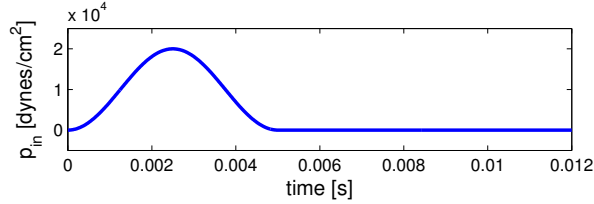


Figure 3: The inlet pressure pulse for Examples 1 and 2. The outlet pressure is kept at 0.

boundary conditions are the absorbing boundary conditions:

$$\frac{\partial \eta_r}{\partial t} - \sqrt{\frac{C_1}{\rho_s}} \frac{\partial \eta_r}{\partial z} = 0 \quad \text{at } z = 0 \quad (32)$$

$$\frac{\partial \eta_r}{\partial t} + \sqrt{\frac{C_1}{\rho_s}} \frac{\partial \eta_r}{\partial z} = 0 \quad \text{at } z = L. \quad (33)$$

To deal with the motion of the fluid domain, the ALE mapping we used in the simulations was defined to be the harmonic extension of the mapping that maps the boundary of  $\Omega$  to the boundary of  $\Omega(t)$  for a given time  $t$ .

Parameter  $\beta$ , introduced in (29), which appears in Step 1 and Step 3 of our numerical scheme was taken to be  $\beta = 1$ . It was numerically observed

in [11] that the change in  $\beta$  is associated with the change in accuracy of the scheme (not the stability), where the value of  $\beta = 1$  provides the highest accuracy for this benchmark problem. We believe that the main reason for the gain in accuracy at  $\beta = 1$  is the strong coupling between the fluid pressure (which incorporates the leading effect of the fluid loading onto the structure) and the structure elastodynamics, which is established for  $\beta = 1$  in Step 3 of the splitting, described above.

*5.1. Example 1:  $\rho_s = 1.1 \text{ g/cm}^3$ .*

We solved the fully nonlinear benchmark problem described above over the time interval  $[0, 0.012]\text{s}$  as in [30]. The numerical results obtained using the kinematically coupled  $\beta$ -scheme were compared with the numerical results obtained using the monolithic scheme by Badia, Quaini and Quarteroni [3, 46]. Figures 4, 5 and 6 show a comparison between tube diameter,

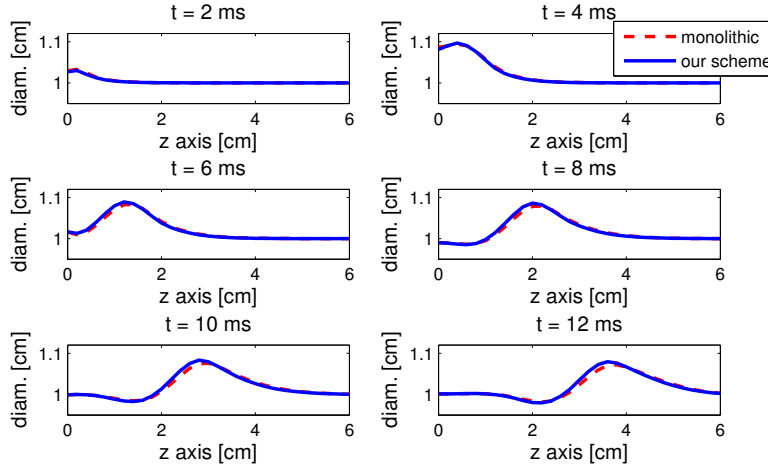


Figure 4: Example 1: Diameter of the tube computed with the kinematically coupled  $\beta$ -scheme (solid line) and with the monolithic scheme used by Quaini in [3, 46] (dashed line). The time step  $\Delta t = 10^{-4}$  is used in both cases.

flowrate and mean pressure, respectively, at six different times. These results were obtained on the same mesh as the one used for the monolithic scheme in [46], containing  $31 \times 11 \mathbb{P}_1$  fluid nodes. More precisely, we used an isoparametric version of the Bercovier-Pironneau element spaces, also known as the

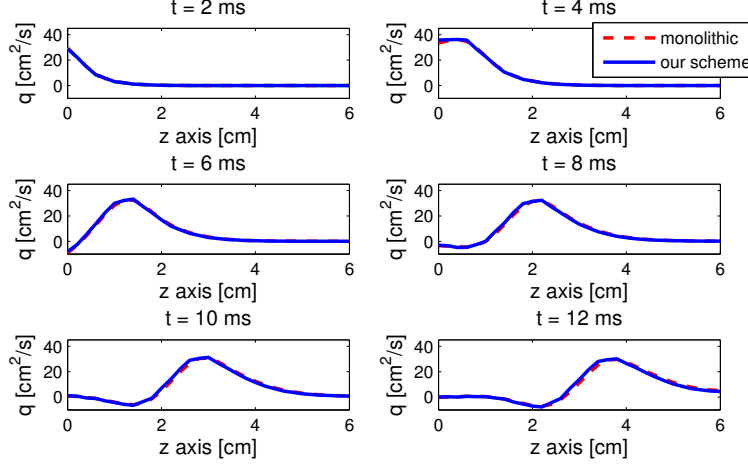


Figure 5: Example 1: Flowrate computed with the kinematically coupled  $\beta$ -scheme (solid line) and with the monolithic scheme used by Quaini in [3, 46] (dashed line). The time step  $\Delta t = 10^{-4}$  in both cases.

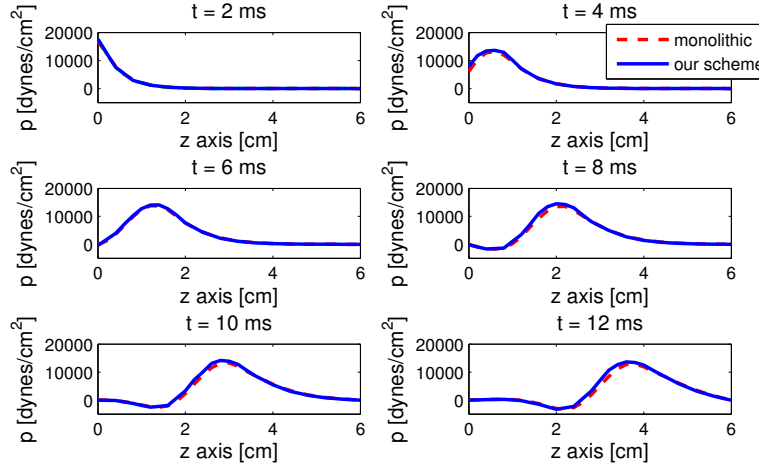


Figure 6: Example 1: Mean pressure computed with the kinematically coupled  $\beta$ -scheme (solid line) and with the monolithic scheme used by Quaini in [3, 46] (dashed line). The time step  $\Delta t = 10^{-4}$  is used in both cases.

$\mathbb{P}_1$ -iso- $\mathbb{P}_2$  approximation in which a coarse mesh is used for the pressure (mesh size  $h_p$ ) and a fine mesh for the velocity (mesh step  $h_v = h_p/2$ ).

The time step used was  $\Delta t = 10^{-4}$  which is the same as the time step used for the monolithic scheme. Due to the splitting error, it is well-known that classical splitting schemes usually require smaller time step to achieve the accuracy comparable to that of monolithic schemes. However, the new splitting with  $\beta = 1$  allows us to use the same time step as in the monolithic method, obtaining comparable accuracy, as shown in [11] and in Figure 7.

The reference solution was defined to be the one obtained with  $\Delta t = 10^{-6}$ . We calculated the relative and absolute  $L^2$  errors for the velocity, pressure and displacement between the reference solution and the solutions obtained using  $\Delta t = 5 \times 10^{-6}, 10^{-5}, 5 \times 10^{-5}$  and  $10^{-4}$ . Table 3 shows the relative error and the convergence rates for the pressure, velocity, and displacement obtained by the kinematically-coupled  $\beta$ -scheme. The graphs in Figure 7 show the absolute error and the convergence in time of the kinematically-coupled  $\beta$ -scheme and the monolithic scheme by Badia, Quaini and Quarteroni [3, 46].

$\Delta t$	$\frac{\ p - p_{ref}\ _{L^2}}{\ p_{ref}\ _{L^2}}$	$L^2$ order	$\frac{\ \mathbf{u} - \mathbf{u}_{ref}\ _{L^2}}{\ \mathbf{u}_{ref}\ _{L^2}}$	$L^2$ order	$\frac{\ \boldsymbol{\eta} - \boldsymbol{\eta}_{ref}\ _{L^2}}{\ \boldsymbol{\eta}_{ref}\ _{L^2}}$	$L^2$ order
$10^{-4}$	0.0251	-	0.0223	-	0.0392	-
$5 \times 10^{-5}$	0.013	1.35	0.0151	0.56	0.0175	1.1
$10^{-5}$	0.0024	1.04	0.0038	0.87	0.0038	0.92
$5 \times 10^{-6}$	0.0011	1.14	0.0017	1.12	0.0017	1.13

Table 3: Example 1: Convergence in time calculated at  $t = 10$  ms.

### 5.2. Example 2: $\rho_s = 0.55 \text{ g/cm}^3$ .

We consider the same test case as in Example 1, but now with the value for the structure density  $\rho_s = 0.55 \text{ g/cm}^3$ . The problem is solved on the time interval  $[0, 0.012]\text{s}$  and with the same mesh as the one used in Example 1. Figures 8, 9 and 10 show the values of the tube diameter, flowrate and mean pressure, respectively, at six different times, obtained with  $\Delta t = 10^{-4}$ .

Finally, to show the convergence of the scheme, we define the reference solution to be the one obtained with  $\Delta t = 10^{-6}$ . We calculated the relative  $L^2$  errors for the velocity, pressure and displacement between the reference solution and the solutions obtained using  $\Delta t = 5 \times 10^{-6}, 10^{-5}, 5 \times 10^{-5}$  and  $10^{-4}$ . Table 4 shows the convergence rates for the pressure, velocity, and displacement obtained by the kinematically-coupled  $\beta$ -scheme. Thus, we see that the scheme performs well for a range of parameters for which

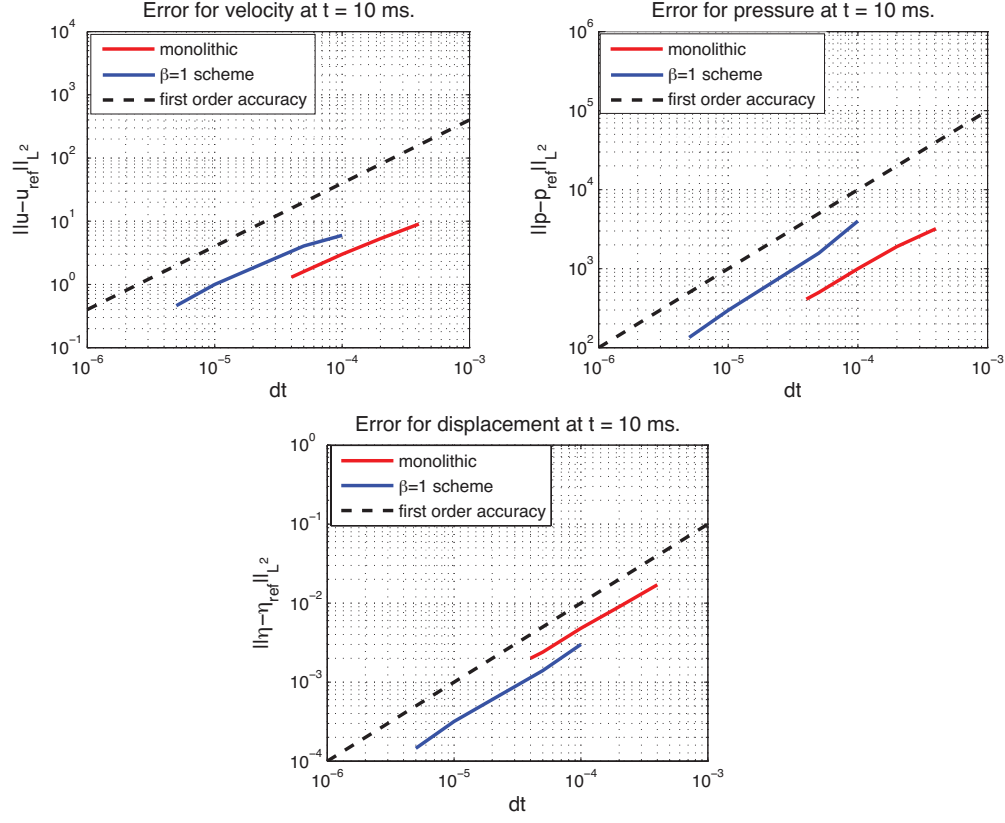


Figure 7: Example 1: The figures show absolute errors compared with the monolithic scheme. Top left: Error for fluid velocity at  $t=10$  ms. Top right: Error for fluid pressure at  $t=10$  ms. Bottom: Error for displacement at  $t=10$  ms, [11]. Both schemes are first-order accurate in time, with comparable accuracy (notice the higher accuracy of the kinematically-coupled  $\beta$  scheme for the displacement).

the classical loosely-coupled, Dirichlet-Neumann scheme is unconditionally unstable.

$\Delta t$	$\frac{\ p-p_{ref}\ _{L^2}}{\ p_{ref}\ _{L^2}}$	$L^2$ order	$\frac{\ u-u_{ref}\ _{L^2}}{\ u_{ref}\ _{L^2}}$	$L^2$ order	$\frac{\ \eta-\eta_{ref}\ _{L^2}}{\ \eta_{ref}\ _{L^2}}$	$L^2$ order
$10^{-4}$	0.0239	-	0.0427	-	0.0749	-
$5 \times 10^{-5}$	0.0096	1.32	0.0286	0.58	0.0408	0.87
$10^{-5}$	0.0017	1.06	0.0067	0.9	0.0079	1.021
$5 \times 10^{-6}$	$7.72e-04$	1.15	0.0031	1.13	0.0035	1.16

Table 4: Example 2: Convergence in time calculated at  $t = 10$  ms.

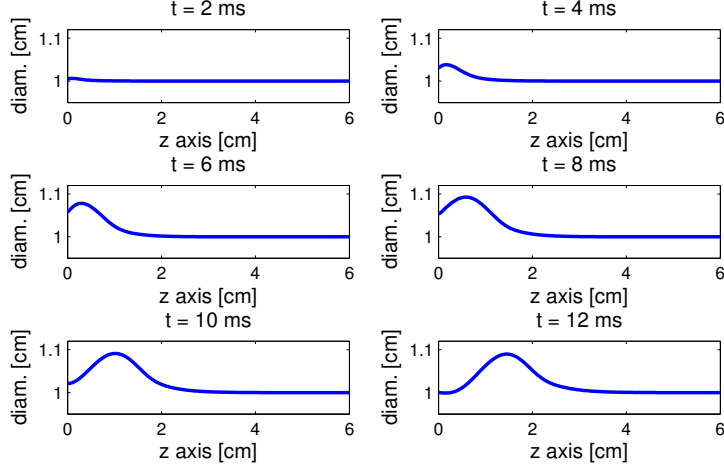


Figure 8: Example 2: Diameter of the tube computed with the kinematically coupled  $\beta$ -scheme, obtained with the time step  $\Delta t = 10^{-4}$ .

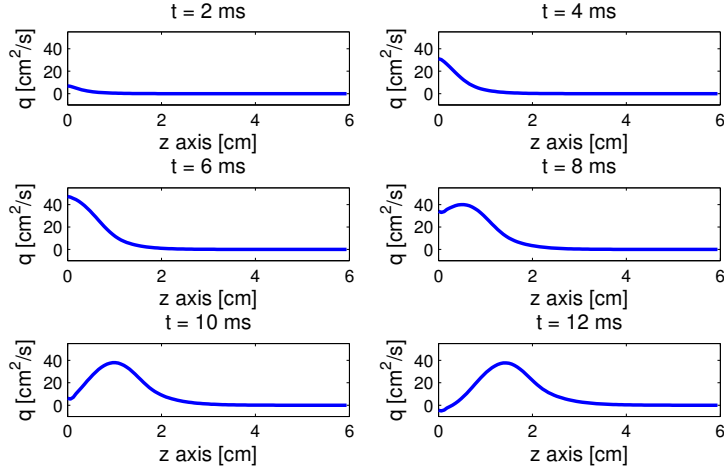


Figure 9: Example 2: Flowrate computed with the kinematically coupled  $\beta$ -scheme, obtained with the time step  $\Delta t = 10^{-4}$ .

## 6. Conclusions

We conclude this manuscript by comparing the kinematically-coupled  $\beta$ -scheme, summarized in (22), with the classical Dirichlet-Neumann scheme

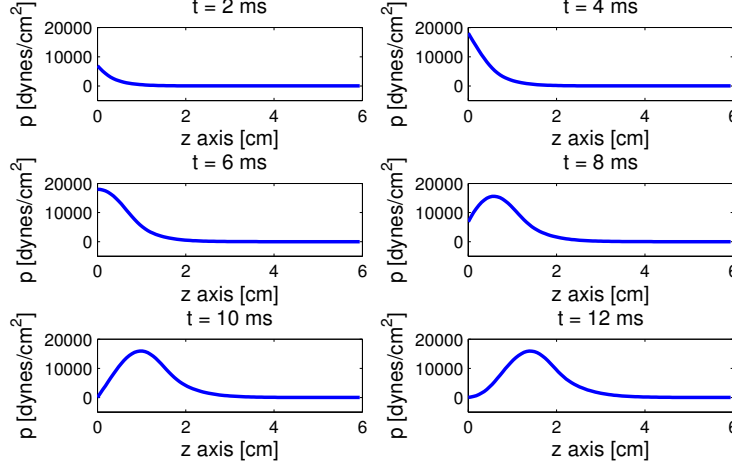


Figure 10: Example 2: Mean pressure computed with the kinematically coupled  $\beta$ -scheme, obtained with the time step  $\Delta t = 10^{-4}$ .

exhibiting the “added mass effect.” Equation (22) can be solved in an implicit way (written with a slight abuse of notation) as:

$$\rho_s h \frac{\partial^2 \eta^{n+1}}{\partial t^2} + \mathcal{L} \eta^{n+1} = \beta(p_{ext}^{n+1} + \mathcal{S}(\beta p^n)). \quad (34)$$

The corresponding equation resulting from the classical Dirichlet-Neumann scheme can be written as follows. We recall that the Dirichlet-Neumann scheme solves the FSI problem (6)-(8) by solving the fluid sub-problem (6) with Dirichlet boundary data for the fluid velocity on  $\Gamma$ , given in terms of the structure velocity  $\partial \eta / \partial t$ , calculated from the previous time step, and then uses the fluid stress, calculated in problem (6), to load the structure in sub-problem (7). Figure 6 shows a block diagram summarizing the main steps.

Using similar ideas as already presented in this manuscript, it was shown in [17] that this kind of partitioned approach leads to solving the problem for  $\eta$  of the form

$$\rho_s h \frac{\partial^2 \eta}{\partial t^2} + \mathcal{L} \eta = p|_{\Gamma}, \quad (35)$$

where

$$p|_{\Gamma} = p_{ext} - \rho_f \mathcal{M}_A \frac{\partial^2 \eta}{\partial t^2}. \quad (36)$$

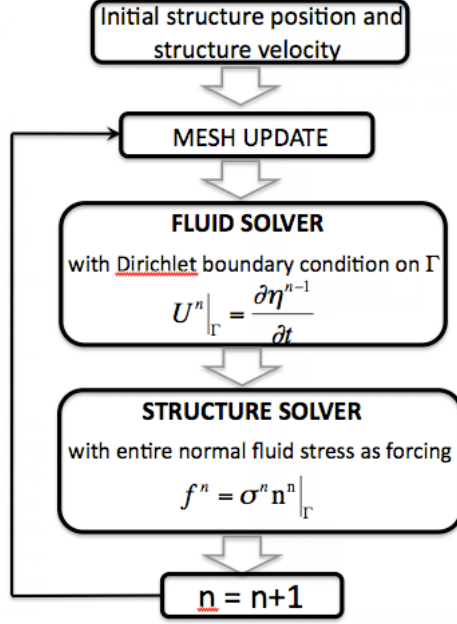


Figure 11: A block diagram showing the main steps of a Dirichlet-Neumann scheme.

Here  $p_{ext}$  comes from the “external” pressure data  $(p_{in/out})$ , and  $\mathcal{M}_A$  is the “added mass operator” introduced in the previous section by formula (25).

While in the Dirichlet-Neumann loosely coupled scheme the  $w$  in the definition of operator  $\mathcal{R}$  (formula (26)) corresponds to the structure inertia  $\partial^2 \eta / \partial t^2$ , in our kinematically coupled  $\beta$ -scheme  $w$  corresponds to the fraction of the fluid stress determined by  $\beta p$ . When  $\beta = 0$ , which corresponds to the original kinematically coupled scheme, this term is zero. We emphasize again that the structure inertia in the kinematically coupled schemes is taken *implicitly* in the Robin boundary condition, and not explicitly, as in the classical loosely coupled schemes.

With the added mass operator the problem for the structure (35) can now be written as

$$(\rho_s h + \rho_f \mathcal{M}_A) \frac{\partial^2 \eta}{\partial t^2} + \mathcal{L} \eta = p_{ext}. \quad (37)$$

Since in the Dirichlet-Neumann loosely coupled partitioned schemes the pressure is calculated in the fluid sub-problem using the structure velocity from the previous time step, this implies that, with a slight abuse of notation, (37)



can be written as

$$\rho_s h \frac{\partial^2 \eta^{n+1}}{\partial t^2} + \rho_f \mathcal{M}_A \frac{\partial^2 \eta^n}{\partial t^2} + \mathcal{L} \eta^n = p_{ext}. \quad (38)$$

More precisely, equation (38) means

$$\rho_s h \frac{\eta^{n+1} - 2\eta^n + \eta^{n-1}}{(\Delta t)^2} + \rho_f \mathcal{M}_A \frac{\eta^n - 2\eta^{n-1} + \eta^{n-2}}{(\Delta t)^2} + \mathcal{L} \eta^n = p_{ext}. \quad (39)$$

It was shown in [17] that this scheme is unconditionally unstable if

$$\frac{\rho_s h}{\rho_f \mu_{max}} < 1, \quad (40)$$

where  $\mu_{max}$  is the maximum eigenvalue of the added mass operator  $\mathcal{M}_A$ . It was also shown in [17] that the maximum eigenvalue  $\mu_{max}$  is associated with the aspect ratio of the fluid domain  $R/L$ . The smaller that aspect ratio (the more slender the domain), the larger the maximum eigenvalue  $\mu_{max}$ .

Going back to equation (34), one can now see that there is no added mass operator associated with the kinematically coupled  $\beta$ -scheme. The right hand side of equation (34) is an iterative procedure which can be written in terms of the initial pressure and of the external (in/out) pressure data. There is no added mass operator  $\mathcal{M}_A$  that appears in (34). Thus, for  $0 \leq \beta \leq 1$ , the kinematically coupled  $\beta$ -scheme does not suffer from the added mass effect for any of the choices of  $\rho_s h$ ,  $\rho_f$ , and domain sizes.

## References

- [1] M. Astorino, F. Chouly, and M.A. Fernández. An added-mass free semi-implicit coupling scheme for fluid-structure interaction. *Comptes Rendus Mathématique*, 347(1-2):99–104, 2009.
- [2] M. Astorino, F. Chouly, and M.A. Fernández Varela. Robin based semi-implicit coupling in fluid-structure interaction: Stability analysis and numerics. *SIAM J. Sci. Comput.*, 31:4041–4065, 2009.
- [3] S. Badia, A. Quaini, and A. Quarteroni. Splitting methods based on algebraic factorization for fluid-structure interaction. *SIAM J. Sci. Comput.* 30(4):7027–7051, 2008.

- [4] S. Badia, A. Quaini, and A. Quarteroni. Coupling Biot and NavierStokes equations for modelling fluidporoelastic media interaction. *J. Comput. Phys.* 228(21):7986–8014, 2009.
- [5] S. Badia, F. Nobile, C. Vergara. Fluid-structure partitioned procedures based on Robin transmission conditions. *J. Comput. Phys.* 227:7027–7051, 2008.
- [6] S. Badia, F.. Nobile, and C. Vergara. Robin-robin preconditioned krylov methods for fluid-structure interaction problems. *Comput. Methods Appl. Mech. Eng.*, 198(33-36):2768–2784, 2009.
- [7] V. Barbu, Z. Grujić, I.a Lasiecka, and A. Tuffaha. Smoothness of weak solutions to a nonlinear fluid-structure interaction model. *Indiana Univ. Math. J.*, 57(3):1173–1207, 2008.
- [8] Y. Bazilevs, V.M. Calo, T.J.R. Hughes, Y. Zhang. Isogeometric fluid-structure interaction: theory algorithms and computations. *Comput. Mech.* 43:3-37, 2008.
- [9] Y. Bazilevs, V.M. Calo, Y. Zhang, T.J.R. Hughes. Isogeometric fluid-structure interaction analysis with applications to arterial blood flow *Comput. Mech.* 38 (4-5): 310–322, 2006.
- [10] H. Beirão da Veiga. On the existence of strong solutions to a coupled fluid-structure evolution problem. *J. Math. Fluid Mech.*, 6(1):21–52, 2004.
- [11] M. Bukač, S. Čanić, R. Glowinski, J. Tambača, and A. Quaini. Fluid-structure interaction in blood flow capturing non-zero longitudinal structure displacement. *J. Comput. Phys.* <http://dx.doi.org/10.1016/j.bbr.2011.03.031>
- [12] M. Bukač, S. Čanić. Longitudinal displacement in viscoelastic arteries: a novel fluid-structure interaction computational model, and experimental validation. *Journal Mathematical Biosciences and Engineering*. Accepted 2012.
- [13] M. Bukač, S. Čanić, B. Muha and A. Quaini. The kinematically-coupled  $\beta$ -scheme for fluid-structure interaction problems with thick elastic structures. In preparation.

- [14] M. Bukač, S. Čanić, B. Muha. The kinematically-coupled  $\beta$ -scheme for fluid-structure interaction problems with multi-layered structures. In preparation.
- [15] E. Burman and M. A. Fernández. Stabilization of explicit coupling in fluid-structure interaction involving fluid incompressibility. *Comput. Methods Appl. Mech. Eng.*, 198:766–784, 2009.
- [16] S. Čanić, J. Tambača, G. Guidoboni, A. Mikelić, C. J. Hartley, and D. Rosenstrauch. Modeling viscoelastic behavior of arterial walls and their interaction with pulsatile blood flow. *SIAM J. Appl. Math.*, 67(1):164–193 (electronic), 2006.
- [17] P. Causin, J. Gerbeau, and F. Nobile. Added-mass effect in the design of partitioned algorithms for fluid-structure problems. *Comput. Methods Appl. Mech. Eng.*, 194(42-44):4506–4527, 2005.
- [18] M. Cervera, R. Codina, M. Galindo. On the computational efficiency and implementation of block-iterative algorithms for nonlinear coupled problems. *Eng. Comput.* 13 (6): 4–30, 1996.
- [19] C. H. Arthur Cheng and Steve Shkoller. The interaction of the 3D Navier-Stokes equations with a moving nonlinear Koiter elastic shell. *SIAM J. Math. Anal.*, 42(3):1094–1155, 2010.
- [20] D. Coutand and S. Shkoller. The interaction between quasilinear elastodynamics and the Navier-Stokes equations. *Arch. Ration. Mech. Anal.*, 179(3):303–352, 2006.
- [21] J. Donea. Arbitrary Lagrangian-Eulerian finite element methods, in: Computational methods for transient analysis. North-Holland, Amsterdam, 1983.
- [22] S. Deparis, M. Fernández, L. Formaggia. Acceleration of a fixed point algorithm for a fluid-structure interaction using transpiration condition. *em Math. Model. Numer. Anal.* 37 (4): 601–616, 2003.
- [23] B. Desjardins, M. J. Esteban, C. Grandmont, and P. Le Tallec. Weak solutions for a fluid-elastic structure interaction model. *Rev. Mat. Comput.*, 14(2):523–538, 2001.

- [24] M. A. Fernández. Incremental displacement-correction schemes for the explicit coupling of a thin structure with an incompressible fluid. *C. R. Math. Acad. Sci. Paris*, 349(7-8):473–477, 2011.
- [25] M. Angel Fernández. Incremental displacement-correction schemes for incompressible fluid-structure interaction: stability and convergence analysis. *Numerische Mathematik*, 2012.
- [26] M.A. Fernández, J.F. Gerbeau, and C. Grandmont. A projection algorithm for fluid-structure interaction problems with strong added-mass effect. *Comptes Rendus Mathématique*, 342(4):279–284, 2006.
- [27] M. Fernández, J.-F. Gerbeau, C. Grandmont. A projection semi-implicit scheme for the coupling of an elastic structure with an incompressible fluid. *Int. J. Numer. Methods Eng.* 69 (4) : 794–821, 2007.
- [28] M. A. Fernández and J. Mullaert. Displacement-velocity correction schemes for incompressible fluid-structure interaction. *C. R. Math. Acad. Sci. Paris*, 349(17-18):1011–1015, 2011.
- [29] C. Figueroa, I. Vignon-Clementel, K.E. Jansen, T. Hughes, C. Taylor. A coupled momentum method for modeling blood flow in three-dimensional deformable arteries. *Comput. Methods Appl. Mech. Eng.* 195: 5685–5706, 2006.
- [30] L. Formaggia, J.F. Gerbeau, F. Nobile, A. Quarteroni. On the coupling of 3D and 1D Navier-Stokes equations for flow problems in compliant vessels. *Comput. Methods Appl. Mech. Eng.*, 191 (6-7):561–582, 2001.
- [31] J. Gerbeau, M. Vidrascu. A quasi-Newton algorithm based on a reduced model for fluid-structure interactions problems in blood flows. *Math. Model. Numer. Anal.* 37 (4):631–648, 2003.
- [32] R. Glowinski. Finite element methods for incompressible viscous flow, in: P.G.Ciarlet, J.-L.Lions (Eds), *Handbook of numerical analysis*, volume 9. North-Holland, Amsterdam, 2003.
- [33] G. Guidoboni, R. Glowinski, N. Cavallini, and S. Čanić. Stable loosely-coupled-type algorithm for fluid-structure interaction in blood flow. *J. Comput. Phys.*, 228(18):6916–6937, 2009.

- [34] P. Hansbo. Nitsches method for interface problems in computational mechanics. *GAMM-Mitt.*, 28(2):183–206, 2005.
- [35] M. Heil. An efficient solver for the fully coupled solution of large-displacement fluid-structure interaction problems. *Comput. Methods Appl. Mech. Eng.* 193: 1–23, 2004.
- [36] T. Hughes, W. Liu, and T. Zimmermann. Lagrangian-Eulerian finite element formulation for incompressible viscous flows. *Comput. Methods Appl. Mech. Eng.*, 29(3):329–349, 1981.
- [37] I. Kukavica and A. Tuffaha. Solutions to a fluid-structure interaction free boundary problem. *DCDS-A*, 32(4):1355–1389, 2012.
- [38] R. van Loon, P. Anderson, J. de Hart, F. Baaijens. A combined fictitious domain/adaptive meshing method for fluid-structure interaction in heart valves. *Int. J. Numer. Meth. Fluids.* 46:533–544, 2004.
- [39] H. Matthies, J. Steindorf. Numerical efficiency of different partitioned methods for fluid-structure interaction. *Z. Angew. Math. Mech.* 2 (80): 557–558, 2000.
- [40] B. Muha and S. Čanić. Existence of a weak solution to a nonlinear fluid-structure interaction problem modeling the flow of an incompressible, viscous fluid in a cylinder with deformable walls. *Arch. Ration. Mech. Anal.*, In print 2012. (DOI) 10.1007/s00205-012-0585-5; FirstOnline Download from: <http://link.springer.com/content/pdf/10.1007%2Fs00205-012-0585-5>
- [41] C.M. Murea and S. Sy. A fast method for solving fluid-structure interaction problems numerically. *Int. J. Numer. Meth. Fl.*, 60(10):1149–1172, 2009.
- [42] F. Nobile. Numerical approximation of fluid-structure interaction problems with application to haemodynamics. PhD Thesis, EPFL, Switzerland, 2001.
- [43] F. Nobile, C. Vergara. An effective fluid-structure interaction formulation for vascular dynamics by generalized Robin conditions. *SIAM J. Sci. Comput.* 30 (2):731–763, 2008.

- [44] C. Peskin. Numerical analysis of blood flow in the heart. *J. Comput. Phys.* 25: 220–252, 1977.
- [45] C. Peskin, D.M. McQueen. A three-dimensional computational method for blood flow in the heart I. Immersed elastic fibers in a viscous incompressible fluid. *J. Comput. Phys.* 81(2): 372–405, 1989.
- [46] A. Quaini. Algorithms for fluid-structure interaction problems arising in hemodynamics. PhD. Thesis, EPFL, Switzerland, 2009.
- [47] A. Quaini and A. Quarteroni. A semi-implicit approach for fluid-structure interaction based on an algebraic fractional step method. *Math. Models Methods Appl. Sci.*, 17(6):957–985, 2007.
- [48] A. Quarteroni, M. Tuveri, and A. Veneziani. Computational vascular fluid dynamics: problems, models and methods. *Computing and Visualization in Science*, 2:163–197, 2000. 10.1007/s007910050039.
- [49] P.L. Tallec, J. Mouro. Fluid-structure interaction with large structural displacements. *Comput. Methods Appl. Mech. Eng.* 190: 3039–3067, 2001.
- [50] S. Zhao, X. Xu, M. Collins. The numerical analysis of fluid-solid interactions for blood flow in arterial structures Part 2: development of coupled fluid-solid algorithms. *Proc. Instn. Mech. Eng. Part H* 212:241–252, 1998.